Available online at www.sciencedirect.com
ScienceDirect
Electrochimica Acta 53 (2007) 1150–1156
ELECTROCHIMICA Acta
www.elsevier.com/locate/electacta

Dithiocarbamate-protected ruthenium nanoparticles: Synthesis, spectroscopy, electrochemistry and STM studies

Wei Chen, Debraj Ghosh, Jia Sun, Moony C. Tong, Fengjun Deng, Shaowei Chen *

Department of Chemistry and Biochemistry, University of California, 1156 High Street, Santa Cruz, CA 95064, USA

Received 10 October 2006; received in revised form 22 January 2007; accepted 27 January 2007
Available online 13 February 2007

Abstract

Stable ruthenium nanoparticles were synthesized in a biphasic system with a protecting monolayer of dithiocarbamate derivatives. The core size of the resulting Ru particles was found to vary with the initial ligand–metal feed ratio. UV–vis spectroscopic measurements showed a Mie scattering profile, with no obvious surface-plasmon resonance. The size and crystal structures of the particles were characterized by transmission electron microscopic (TEM) measurements. A significant fraction of the nanoparticles was found within the size range of 2–4 nm in diameter and of spherical shape from the TEM measurements. Clear lattice fringes could be observed in high-resolution TEM images with the fringe spacing consistent with the Ru(1 0 1) lattice planes. Electrochemical studies of Ru particles with different core size exhibited the solution-phase quantized charging of the particle double layers, analogous to those reported for gold and other transition-metal particles. The potential spacing between adjacent quantized charging peaks was found to vary with the particle core size, corresponding to the variation of the particle molecular capacitance. These charge-transfer properties were very consistent with the STM measurements of isolated nanoparticles which exhibit clear Coulomb blockade and staircase features.
© 2007 Published by Elsevier Ltd.

Keywords: Ruthenium nanoparticle; Dithiocarbamate; Quantized charging; Coulomb blockade; TEM; STM

1. Introduction

It has been very well documented that owing to the quantum mechanical effects, metal nanoparticles in the size range of 1–10 nm display electronic structures that render their physical and chemical properties different from those of bulk metals and molecular compounds [1,2]. Numerous protocols have been developed for the synthesis of novel functional nanomaterials. Of these, the biphasic method reported by Brust et al. [3] represents an effective route to the preparation of organically capped metal nanoparticles. In this synthetic protocol, a metal salt precursor is reduced into metallic form by a strong reducing agent in the presence of appropriate surfactant ligands. The dimension and structure of the resulting nanoparticles is the combined consequence of at least two competing processes [4], nucleation of zero-valence metals in the formation of the particle cores and passivation of the surfactant molecules onto the core surface that impede the growth of the particles. A variety of nanoparticles have been prepared, e.g., Au [5–7], Pt [8–10], Pd [11–13], Ag [14–16], Cu [17–20], and even alloys [21,22]. In addition, while alkanethiols have been commonly used as the ligands of choice in the stabilization of the nanoparticles because of their strong affinity to transition metal surfaces forming metal–thiolate (M–S) bonds, other surfactant molecules with unique functional groups have also been used, for instance, isocyanide derivatives have been used to prepare stable Pt nanoparticles [23]; Au and Ag nanoparticles have also been prepared by a protecting monolayer of arenethiols [24] and dithiocarbamates [25], respectively. More recently, it was reported that diazonium [26] and diazo [27] derivatives could also be used to stabilize nanoparticles by the formation of metal–carbon linkages. The diverse nature of the particle surface protecting layers can then be exploited for the ready control of the

* Corresponding author. Tel.: +1 831 459 5841; fax: +1 831 459 2935.
E-mail address: schen@chemistry.ucsc.edu (S. Chen).

0013-4686/$ – see front matter © 2007 Published by Elsevier Ltd.
doi:10.1016/j.electacta.2007.01.082

physical and chemical properties of the resulting nanoparticle materials.

One of the unique properties of these organically capped nanoparticle is the quantized charging to the particle molecular capacitance [11,28–30]. With nanometer-sized cores and low dielectric protecting shells, the particles exhibit a molecular capacitance (C_{MPC}) of the order of attofarad (aF), which renders the energetic barrier for a single electron transfer ($e^2/2C_{MPC}$) greater than the thermal kinetic energy (k_BT). Such behaviors have been observed in STM measurements of isolated nanoparticles, resulting in the so-called Coulomb staircase charging [31]. In solutions, a series of well-defined voltammetric waves can be observed which are ascribed to the discrete charging to the particle double-layer capacitance [30]. Moreover, it has been found that when the MPC dimensions decrease, the charging features exhibit a transition from bulk double-layer charging to molecular-like redox behaviors [30]. It should be noted that most of the work on electrochemical quantized charging has been focused on Au nanoparticles thus far. More recently, similar responses were also observed with Pd [11,12,32], Cu [17], and Ag [25] particles, thanks to the rapid advance in the synthetic end where ultrasmall nanoparticles now become readily available.

In this paper, a series of dithiocarbamate-protected ruthenium nanoparticles were prepared by the modified Brust protocol [3]. Ruthenium is well renowned for their catalytic activities. For instance, Ru–Pt alloys have been found to be the most effective electrocatalysts used in direct methanol fuel cells [33]. Thus, an understanding of their electron transfer properties is of critical importance in the optimization of their applications in these diverse electrocatalytic reaction processes. Several chemical methods have been reported for the preparation of ruthenium nanoparticles, for instance, by the reduction of ruthenium salts in water with a strong reducing agent at room temperature [34] or by thermolysis in refluxing alcohols [35–37]. In the thermolysis route, it was observed that highly monodisperse Ru nanoparticles could be obtained with the particle core size controlled by the refluxing temperature and the concentration of the stabilizing ligands. However, the resulting Ru nanoparticles were found to be insoluble in a number of common organic solvents and the Ru nanoparticles tended to agglomerate after extensive rinsing, rendering it difficult for further investigations.

In order to overcome this problem, in a recent study [27], we found that by using diazo derivatives which exhibited a strong affinity to freshly prepared Ru surfaces forming Ru-carbene π bonds, the resulting Ru nanoparticles could then be transferred to an organic phase (e.g., toluene, hexane and dichlomethane) and they were stable for an extended period of time without apparent variation of the structure and properties. In this paper, we described a complementary approach based on the modified Brust protocol [3] to prepare stable Ru nanoparticles by the passivation of dithiocarbamate derivatives. This is partly motivated by the strong chemisorption of the bidentate moieties on transition metal surfaces [38], which is anticipated to further stabilize the resulting particles and helps reduce the particle dimensions during the particle growth, as observed recently in the synthesis of nanometer-sized Au [38,39] and Ag [25] nanoparticles. Our focus here will be on the optical and electrochemical properties of these functional nanomaterials.

2. Experimental section

2.1. Chemicals

Ruthenium chloride ($RuCl_3$, 99+%, ACROS), sodium borohydride ($NaBH_4$, 99+%, ACROS), tetraoctylammonium bromide (TOABr, 98%, Aldrich), carbon disulfide (CS_2, Fisher Scientific, spectroanalyzed), and didecylamine (98%, Aldrich) were all used as received. Tetrabutylammonium perchlorate (TBAP, 98%, ACROS) was recrystallized twice prior to use. All solvents were obtained from typical commercial sources and were used without further treatment except for CH_2Cl_2, which was freshly distilled prior to use. Water was supplied by a Barnstead Nanopure water system (18.3 MΩ).

2.2. Synthesis of ruthenium nanoparticles

The method to prepare didecylamine dithiocarbamate (DTC10) has been described by Zhao et al. [38]. Briefly, a 10 wt% solution of CS_2 was prepared in ethanol, in which one molar equivalent of didecylamine dissolved in ethanol was added dropwise under magnetic stirring for 1 min. DTC10 protected Ru nanoparticles (Ru-DTC10) were then synthesized according to the modified Brust reaction [3], which was summarized in Scheme 1. In a typical reaction, 0.5 mmol $RuCl_3$ was first dissolved in 0.5 M HCl under vigorous stirring (forming $RuCl_4^-$ complexes). A total of 50 ml of toluene with 1.1 g of TOABr was then added into the solution where the $RuCl_4^-$ ions were transferred from the aqueous phase to the organic phase after 30 min of stirring. The aqueous phase was removed and a calculated amount of DTC10 ligands was added in a dropwise fashion into the solution. The solution was stirred for about 20 min in an ice bath and then 0.39 g of $NaBH_4$ dissolved in 20 ml H_2O was added quickly into the solution. The solution color changed rapidly from dark red to dark green and then to dark brown. The color change signified that Ru(III) (dark red) was finally reduced to Ru(0) (dark brown), in consistence with previous observations in the preparation of ruthenium nanoparticles [34–37]. The solution was stirred for 30 min in the ice bath and then at room temperature overnight. The toluene phase was then collected and dried in a rotary evaporator. The Ru particles were washed several times with Nanopure water and methanol, and then redissolved in dichloromethane (CH_2Cl_2).

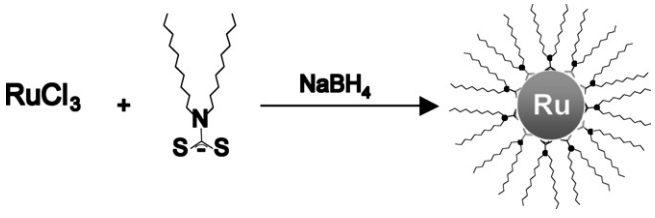

Scheme 1. Synthetic procedure of DTC-stabilized ruthenium nanoparticles.

The resulting solution was stirred overnight and a transparent Ru colloid dispersed in CH_2Cl_2 was obtained without precipitation. The resulting Ru-DTC10 nanoparticles were very stable in apolar organic solvents even after extensive washing by water and methanol. Three batches of particles were prepared with the initial feed ratio of Ru to DTC10 varied from 1:3, 1:1.5 to 1:0.75. The resulting particles were therefore denoted as Ru-DTC10 (3×), (1.5×), and (0.75×), respectively.

The purity of the particles was then examined by using proton NMR spectroscopy (Varian Unity 500 MHz) with concentrated solutions of the particles dissolved in $CDCl_3$. The lack of sharp features indicated the absence of free ligands.

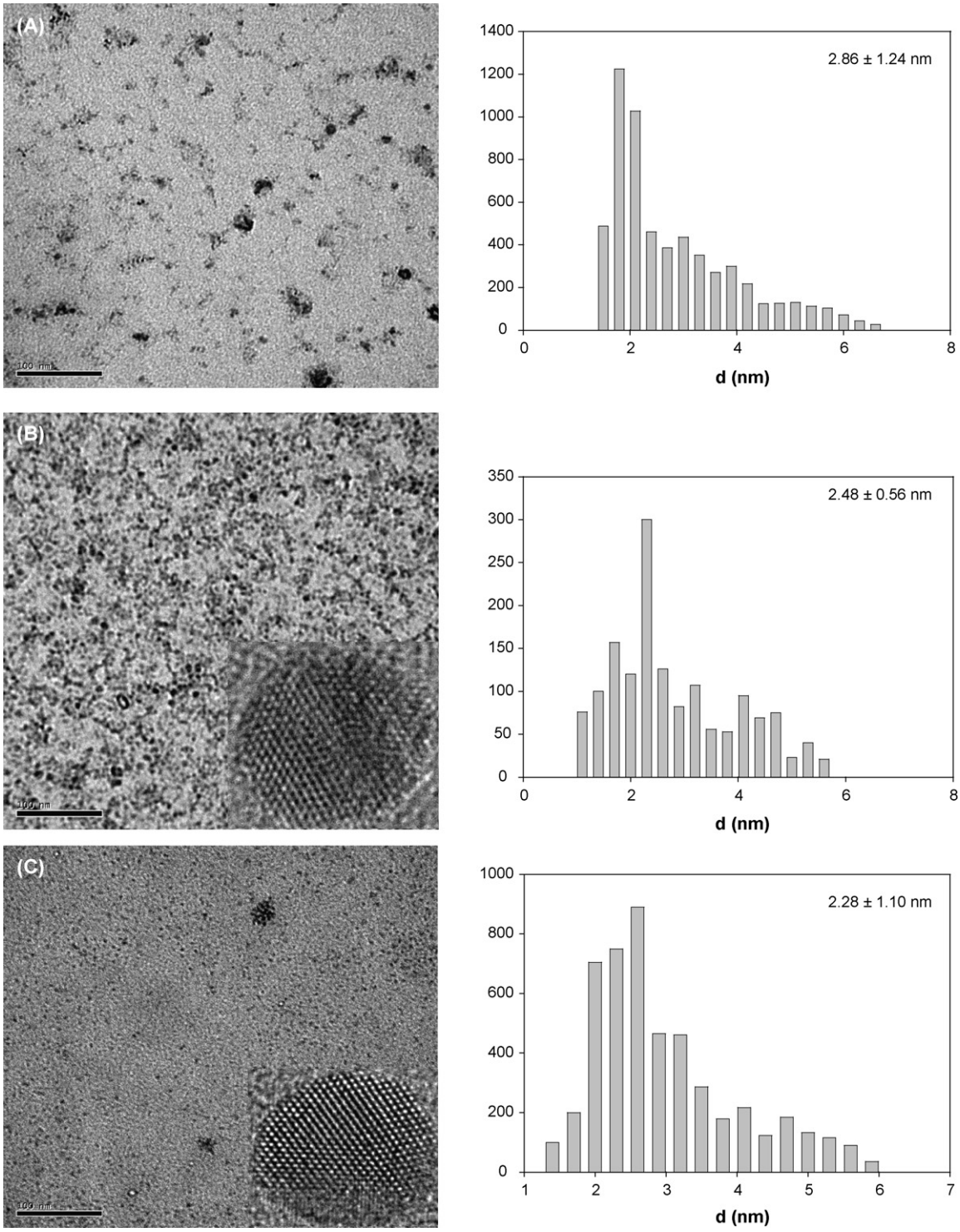

Fig. 1. Transmission electron micrographs of Ru-DTC10 nanoparticles: (A) (0.75×); (B) (1.5×); (C) (3×). Insets show the corresponding high-resolution transmission electron micrographs. The corresponding core diameter histograms are shown to the right. The scale bars are all 100 nm.

2.3. Spectroscopies

Particle core size was measured with a JEOL 1200 EX transmission electron microscope (TEM), a Philips CM200/FEG high-resolution transmission electron microscope (HRTEM). In these measurements, the samples were prepared by casting a drop of the particle solution in hexane onto a 200-mesh Formvar-coated copper grid. The particle size was measured by using ImageJ analysis of the TEM micrographs. UV–vis spectroscopic studies were performed with an ATI Unicam UV4 spectrometer using a 1-cm quartz cuvette with a resolution of 2 nm.

2.4. Electrochemistry

Voltammetric measurements were carried out with a CHI 440 electrochemical workstation. A polycrystalline gold disk electrode (sealed in a glass tubing) was used as the working electrode. A Ag/AgCl wire and a Pt coil were used as the reference and counter electrodes, respectively. The gold electrode was first polished with alumina slurries of 0.05 μm and then cleansed by sonication in 0.1 M HNO_3, H_2SO_4 and Nanopure water successively. Before each measurement the electrolyte solution was deaerated by bubbling ultra-high-purity N_2 for 20 min and protected with a nitrogen atmosphere during the entire experiments.

2.5. STM studies

STM measurements were performed with an Agilent PicoLE microscope, operated at room temperature in air. Atomically flat Au(1 1 1) substrates were first prepared by thermal evaporation onto a freshly cleaved mica at 350 °C in vacuo (10^{-7} Torr). The gold film, about 150 nm in thickness, was cooled down to room temperature before being removed out of the deposition chamber. Then the Au substrate was immersed into 1 mM decanethiol in ethanol for 24 h, followed by rinsing with copious amount of ethanol and blow-drying in a gentle stream of nitrogen. The particles were deposited onto the substrate surface using the dropcast method. The intercalation between the alkyl chains of the self-assembled monolayers and the dithiocarbamate ligands helped immobilize the particles and thus minimize the drifting in STM measurements [40]. A mechanically cut Pt/Ir tip was used in STM measurements. STM images were recorded in constant current mode. *I–V* data were collected in the spectroscopy mode by parking the tip on top of selected particles when the feedback loop was turned off. One hundred *I–V* data points were collected in a typical voltage range of ±2 V. Every *I–V* curve was averaged for five times.

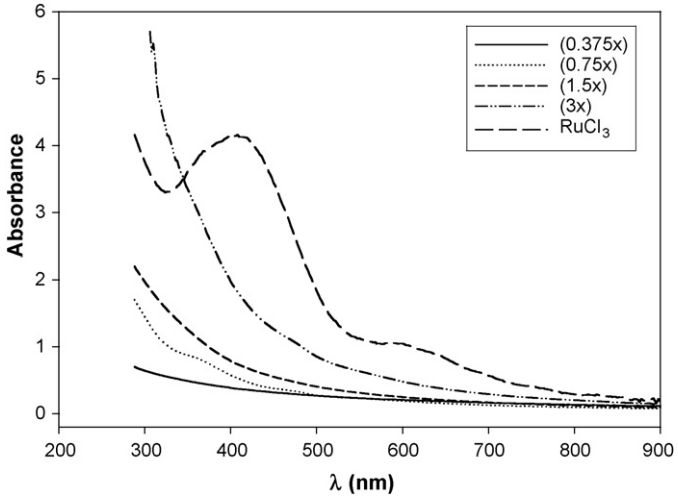

Fig. 2. UV–vis absorption spectra of the varied ruthenium nanoparticles and the precursor $RuCl_3$. Ruthenium particles were dissolved in CH_2Cl_2 with a concentration of ca. 0.1 mg/ml; whereas the $RuCl_3$ solution was prepared at 5 mM in water.

3. Results and discussion

3.1. Ruthenium nanoparticles

TEM has been a powerful tool in the determination of nanoparticle dimensions and structures. Fig. 1 shows the TEM

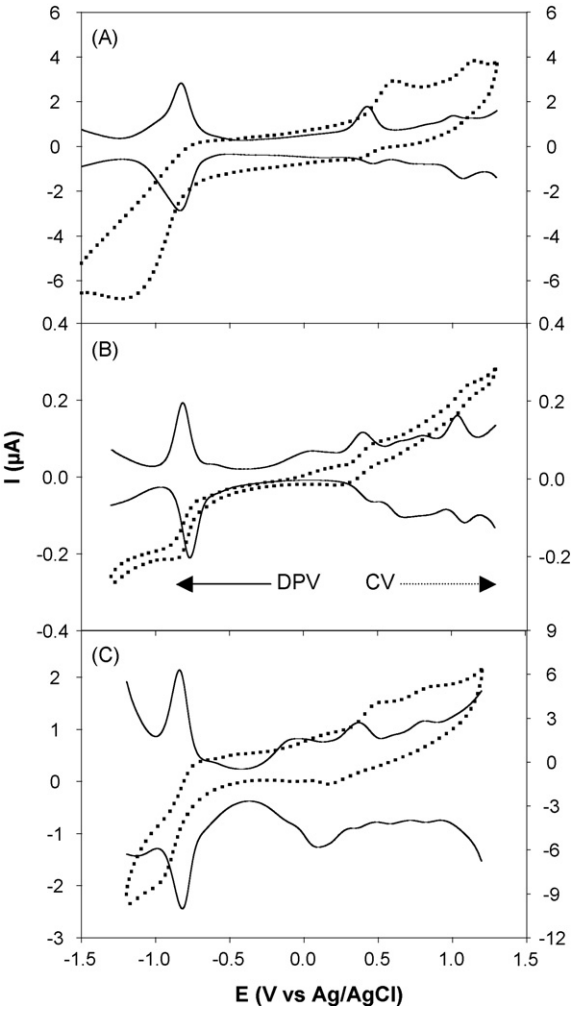

Fig. 3. CV and DPV of Ru-DTC10 particles of different sizes: (A) 2.86 ± 1.24 nm; (B) 2.48 ± 0.56 nm; (C) 2.28 ± 1.1 nm. All the particles were dissolved in CH_2Cl_2 at a concentration of 4 mg/ml with 0.1 M TBAP at an Au working electrode (1.6 mm^2). CV potential scan rate 0.1 V/s. In DPV, potential scan rate 10 mV/s, pulse amplitude 50 mV, pulse width 50 ms, pulse period 200 ms, and sample width 17 ms.

and HRTEM micrographs of the varied Ru-DTC10 particles along with the corresponding size histograms. From the TEM images, we can see that in general, the prepared Ru nanoparticles exhibit spherical shapes with the majority of the particles falling within the range of 2–4 nm in diameter. Additionally, the particle core size exhibit a slight decrease with increasing DTC to Ru feed ratio: (0.75×), 2.86 ± 1.24 nm; (1.5×), 2.48 ± 0.56 nm; (3×), 2.28 ± 1.1 nm. This is similar to the observation with gold nanoparticles which are passivated by alkanethiolates [41]. Yet, the core size distribution is somewhat broader than that observed with Ru particles prepared by the thermolysis route [35–37]. From HRTEM images, the crystal structures of the Ru-DTC10 nanoparticles were also examined (shown as the corresponding insets). In the Fig. 1C inset, very clear lattice fringes can be observed, and the fringe spacing is found to be approximately 0.206 nm, in good agreement with the space between the Ru(1 0 1) lattice planes. This suggests that the nanoparticles are of single crystal ruthenium. In addition, twin structures can also be seen in the HRTEM image (e.g., Fig. 1B inset). The two fringe spacings are 0.206 and 0.232 nm, corresponding to the Ru(1 0 1) and Ru(1 0 0) lattice planes. Similar observations have been reported previously [42].

Fig. 2 shows the UV–vis spectra of the ruthenium nanoparticles in dichloromethane (also included was the spectrum for the precursor ($RuCl_3$) in water). It can be seen that for ruthenium colloidal solutions, the UV–vis spectra exhibit a typical Mie exponential decay profile with no obvious absorption peak, in consistence with earlier studies [27], whereas the original precursor ($RuCl_3$) shows a broad absorption peak at about 407 nm which can be attributable to the ligand–metal charge transfer. These measurements further confirm that the Ru(III) ions are completely reduced to zero-valence ruthenium forming the nanoparticles.

3.2. Electrochemistry

With the nanoparticle core size averaged between 2 and 3 nm, it is anticipated that the particles in solution will exhibit the electrochemical quantized charging characteristics [43]. Fig. 3 shows the cyclic (CV) and differential pulse voltammograms (DPV) of Ru-DTC10 particles of different sizes in dichloromethane (DCM) containing 0.1 M TBAP. It can be seen that for all particles, there are a series of voltammetric peaks within the potential range of −1.5 to +1.5 V. These are ascribed to the quantized charging to the particle molecular capacitance, Yet, they are less clearly defined than those observed previously with highly monodisperse carbene-functionalized ruthenium nanoparticles [27]. From the potential spacing (ΔV) between the adjacent charging peaks in DPV, the capacitance C_{MPC} of the Ru nanoparticles can be evaluated by $C_{MPC} = e/\Delta V$, where e is the electronic charge. Table 1 summarizes the anodic and cathodic peak potentials, peak spacing and the capacitance of the varied ruthenium nanoparicles. It can be seen that the capacitance of the Ru nanoparticles decreases somewhat with decreasing core size. For instance, the three representative samples shown in Fig. 3 exhibit a particle capacitance of 0.537 aF (2.86 nm, 0.75×), 0.507 aF (2.48 nm, 1.5×), and 0.468 aF (2.28 nm, 3×), respectively. In addition, from Table 1 it can be seen that the typical peak splitting (ΔE_p) is smaller than 100 mV, indicating kinetically (quasi) reversible electron transfer reactions, akin to the observations with gold nanoparticles [30].

3.3. STM measurements

The nanoparticle single electron transfer properties have also been examined in STM measurements. Fig. 4 (left panels) depicts two representative STM images of isolated Ru-DTC10

Table 1
Formal potentials and capacitance of Ru-DTC10 nanoparticles[a]

Core size (nm)[b]	$E_{p,c}$ (V)[c]	$E_{p,a}$ (V)[c]	E_p (V)[c]	ΔE_p (V)[c]	ΔV_c (V)[c]	C_{MPC} (aF)[d]
2.86 ± 1.24	−0.863	−0.828	−0.846	0.035		
	0.464	0.424	0.444	0.040	1.290	
	0.724	0.816	0.770	0.092	0.326	0.537
	1.072	1.008	1.040	0.064	0.270	
2.48 ± 0.56	−0.870	−0.820	−0.845	0.050		
	−0.530	−0.560	−0.545	0.031	0.300	
	−0.233	−0.202	−0.218	0.031	0.327	0.507
	0.097	0.089	0.093	0.008	0.311	
	0.450	0.386	0.418	0.064	0.325	
	0.97	0.99	0.98	0.020	0.565	
2.28 ± 1.10	−0.925	−0.940	−0.933	0.015		
	0.132	0.102	0.117	0.030	1.050	
	0.450	0.404	0.427	0.046	0.310	0.468
	0.808	0.794	0.801	0.014	0.374	

[a] Peak positions were derived from differential pulse voltammetry (DPV) in Fig. 3.
[b] Core size of the particles were determined by the TEM images in Fig. 1.
[c] Subscripts (a and c) denote anodic and cathodic peaks, $E_p = (E_{p,a} + E_{p,c})/2$, $\Delta E_p = |E_{p,a} - E_{p,c}|$, ΔV_C is the peak spacing between two adjacent peaks.
[d] Particle capacitances were evaluated from the average ΔV_C ($\Delta V_C = e/C$).

(1.5×) nanopaticles deposited on a decanethiol self-assembled monolayer on a Au(1 1 1) surface in air. At a bias voltage of 1.5 V and a small set point current of 20 pA, stable images of the particles were acquired at increased distance between the tip and the sample [40,44]. Two isolated nanoparticles (labels A and B) were selected, and lateral sizes of 6.0 and 8.5 nm were determined by the line profiles across the particles, which may be approximated as the particle core diameter plus two dithiocarbamate ligand chain lengths. As the chain length of the dithiocarbamate ligand can be estimated to be 1.4 nm by Hyperchem®, the corresponding diameter of the two particles is 5.7 nm (particle A) and 3.2 nm (particle B), respectively.

The corresponding *I–V* and d*I*/d*V* curves of these two Ru nanoparticles were shown in Fig. 4 (right panels). For the "A" particle, the tunneling current was close to zero when the voltage bias varied from −0.40 to +0.40 V. Beyond this voltage range, several current steps can be seen with almost even potential spacing of 0.4 V between adjacent current steps. For the smaller particle "B", the tunneling spectroscopic measurements showed a featureless region within the voltage range of −0.8 to +0.8 V. Beyond this, some current steps can also be seen. Yet, the potential spacing between adjacent current steps are found to vary from 0.4 to 0.5 V. Furthermore, the *I–V* spectrum exhibits an asymmetric shape between the currents in the negative and positive biases. It should be mentioned that when the STM tip was parked directly on the SAM surface, only featureless responses were found in the corresponding *I–V* measurements.

The above measurements indicate that both Coulomb blockcade and staircase features were observed with nanosized Ru particles; and the Coulomb blockade gap increases with decreasing diameter of the Ru nanoparticles. For ultrasmall Ru nanoparticle, the large Coulomb blockade suggests the evolution of a significantly quantized electronic structure, for example, the appearance of a substantial gap between the highest occupied and lowest unoccupied orbitals in the particle [30]. The observed asymmetry observed with the smaller particle might be ascribed to the nonzero residual charge residing on the particle [45].

For particle aggregates, the corresponding *I–V* measurements typically exhibit (almost) linear responses, most likely arising from the strong electronic coupling between adjacent particles thanks to the close proximity of the particles.

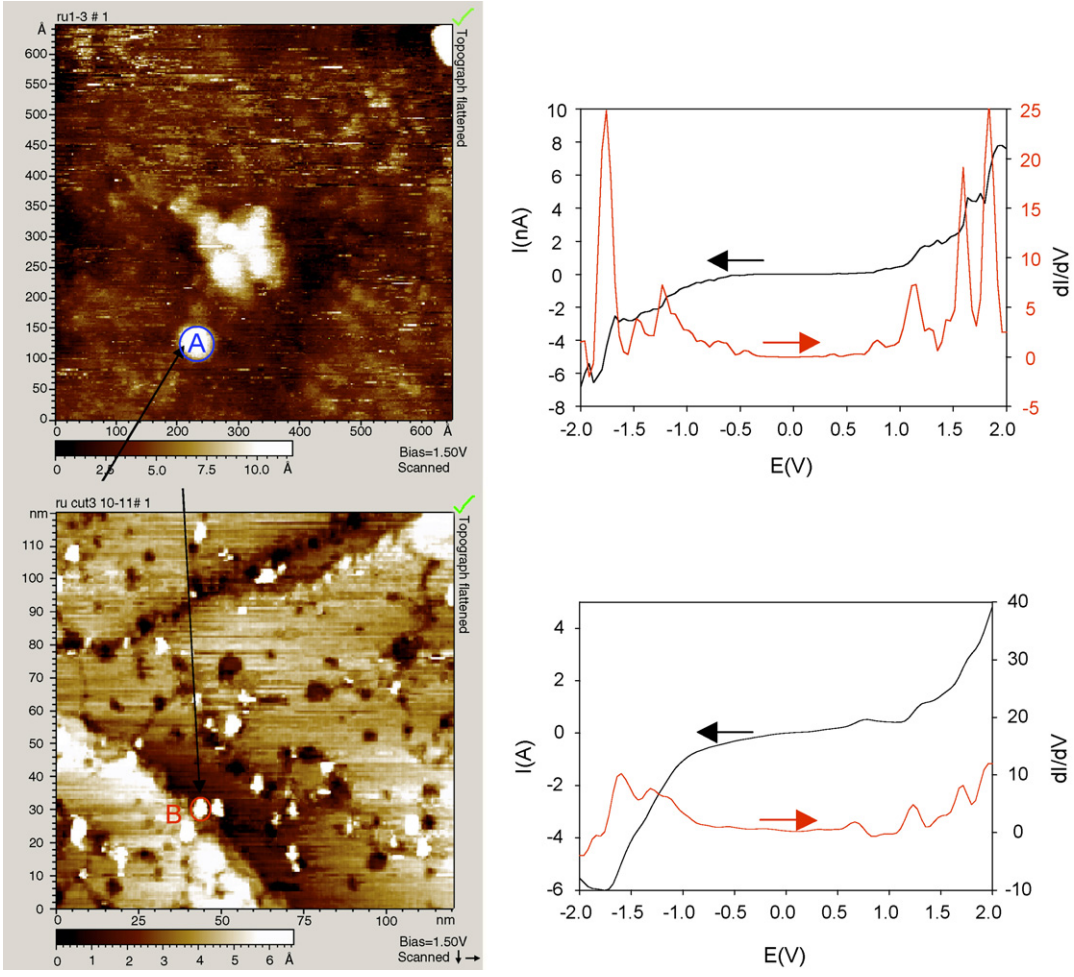

Fig. 4. STM images (constant current mode) and scanning tunneling spectroscopy of Ru nanoparticle deposited on decanethiol self-assembled monolayers/Au(1 1 1) at room temperature. The left panels are STM images acquired at $I = 20$ pA and bias = 1.5 V. The right panels are the corresponding *I–V* and d*I*/d*V* profiles for the two particles labeled as "A" and "B" to the left. The initial set point is 1.5 V and 50 pA.

4. Summary

In this study, a series of dithiocarbamate-passivated ruthenium nanoparticles were synthesized by using the modified Brust protocol where the particle core size was found to increase with decreasing feed ratio of the dithiocarbamate ligand to the ruthenium salt precursor. UV–vis spectroscopic measurements showed a Mie scattering profile, with no obvious surface-plasmon resonance. TEM measurements indicated that a rather large fraction of the particles was within the range of 2–4 nm in diameter. In high-resolution TEM measurements, the lattice fringes were found to be consistent with the Ru(1 0 1) lattice planes. In electrochemical measurements, quantized capacitance (Coulomb staircase) charging was observed, and the particle capacitance evaluated from the peak spacings between adjacent charging peaks was found to increase with increasing particle size, similar to the behaviors with gold nanoparticles. Such observations were also consistent with STM measurements of individual nanoparticles where the current–potential (I–V) profiles varied with the particle dimensions.

Acknowledgments

This work was supported in part by the NSF (CAREER Award CHE-0456130), ACS–PRF (39729-AC5M), and UC Energy Institute.

References

[1] A.P. Alivisatos, Science 271 (1996) 933.
[2] M.C. Daniel, D. Astruc, Chem. Rev. 104 (2004) 293.
[3] M. Brust, M. Walker, D. Bethell, D.J. Schiffrin, R. Whyman, J. Chem. Soc. Ser. Chem. Commun. (1994) 801.
[4] S.W. Chen, A.C. Templeton, R.W. Murray, Langmuir 16 (2000) 3543.
[5] R. Guo, D. Georganopoulou, S.W. Feldberg, R. Donkers, R.W. Murray, Anal. Chem. 77 (2005) 2662.
[6] V.L. Jimenez, D.G. Georganopoulou, R.J. White, A.S. Harper, A.J. Mills, D.I. Lee, R.W. Murray, Langmuir 20 (2004) 6864.
[7] Y. Joseph, I. Besnard, M. Rosenberger, B. Guse, H.G. Nothofer, J.M. Wessels, U. Wild, A. Knop-Gericke, D.S. Su, R. Schlogl, A. Yasuda, T. Vossmeyer, J. Phys. Chem. B 107 (2003) 7406.
[8] W.X. Tu, K. Takai, K. Fukui, A. Miyazaki, T. Enoki, J. Phys. Chem. B 107 (2003) 10134.
[9] C. Yee, M. Scotti, A. Ulman, H. White, M. Rafailovich, J. Sokolov, Langmuir 15 (1999) 4314.
[10] S.E. Eklund, D.E. Cliffel, Langmuir 20 (2004) 6012.
[11] S.W. Chen, K. Huang, J.A. Stearns, Chem. Mater. 12 (2000) 540.
[12] F.P. Zamborini, S.M. Gross, R.W. Murray, Langmuir 17 (2001) 481.
[13] C.K. Yee, R. Jordan, A. Ulman, H. White, A. King, M. Rafailovich, J. Sokolov, Langmuir 15 (1999) 3486.
[14] K.V. Sarathy, G. Raina, R.T. Yadav, G.U. Kulkarni, C.N.R. Rao, J. Phys. Chem. B 101 (1997) 9876.
[15] S.T. He, J.N. Yao, P. Jiang, D.X. Shi, H.X. Zhang, S.S. Xie, S.J. Pang, H.J. Gao, Langmuir 17 (2001) 1571.
[16] M.J. Rosemary, T. Pradeep, J. Colloid Interf. Sci. 268 (2003) 81.
[17] S.W. Chen, J.M. Sommers, J. Phys. Chem. B 105 (2001) 8816.
[18] M. Aslam, G. Gopakumar, T.L. Shoba, I.S. Mulla, K. Vijayamohanan, S.K. Kulkarni, J. Urban, W. Vogel, J. Colloid Interf. Sci. 255 (2002) 79.
[19] T.P. Ang, T.S.A. Wee, W.S. Chin, J. Phys. Chem. B 108 (2004) 11001.
[20] T.Y. Dong, H.H. Wu, M.C. Lin, Langmuir 22 (2006) 6754.
[21] T.P. Ang, W.S. Chin, J. Phys. Chem. B 109 (2005) 22228.
[22] X. Gao, K. Tam, K.M.K. Yu, S.C. Tsang, Small 1 (2005) 949.
[23] S.L. Horswell, C.J. Kiely, I.A. O'Neil, D.J. Schiffrin, J. Am. Chem. Soc. 121 (1999) 5573.
[24] S.W. Chen, R.W. Murray, Langmuir 15 (1999) 682.
[25] M.C. Tong, W. Chen, J. Sun, D. Ghosh, S.W. Chen, J. Phys. Chem. B 110 (2006) 19238.
[26] F. Mirkhalaf, J. Paprotny, D.J. Schiffrin, J. Am. Chem. Soc. 128 (2006) 7400.
[27] W. Chen, J.R. Davies, D. Ghosh, M.C. Tong, J.P. Konopelski, S. Chen, Chem. Mater. 18 (2006) 5253.
[28] S.W. Chen, J. Electroanal. Chem. 574 (2004) 153.
[29] A.C. Templeton, M.P. Wuelfing, R.W. Murray, Acc. Chem. Res. 33 (2000) 27.
[30] S.W. Chen, R.S. Ingram, M.J. Hostetler, J.J. Pietron, R.W. Murray, T.G. Schaaff, J.T. Khoury, M.M. Alvarez, R.L. Whetten, Science 280 (1998) 2098.
[31] R.S. Ingram, M.J. Hostetler, R.W. Murray, T.G. Schaaff, J.T. Khoury, R.L. Whetten, T.P. Bigioni, D.K. Guthrie, P.N. First, J. Am. Chem. Soc. 119 (1997) 9279.
[32] Y.G. Kim, J.C. Garcia-Martinez, R.M. Crooks, Langmuir 21 (2005) 5485.
[33] H.S. Liu, C.J. Song, L. Zhang, J.J. Zhang, H.J. Wang, D.P. Wilkinson, J. Power Sources 155 (2006) 95.
[34] J. Yang, J.Y. Lee, T.C. Deivaraj, H.P. Too, J. Colloid Interf. Sci. 271 (2004) 308.
[35] S. Gao, J. Zhang, Y.F. Zhu, C.M. Che, New J. Chem. 24 (2000) 739.
[36] N. Chakroune, G. Viau, S. Ammar, L. Poul, D. Veautier, M.M. Chehimi, C. Mangeney, F. Villain, F. Fievet, Langmuir 21 (2005) 6788.
[37] G. Viau, R. Brayner, L. Poul, N. Chakroune, E. Lacaze, F. Fievet-Vincent, F. Fievet, Chem. Mater. 15 (2003) 486.
[38] Y. Zhao, W. Perez-Segarra, Q.C. Shi, A. Wei, J. Am. Chem. Soc. 127 (2005) 7328.
[39] M.S. Vickers, J. Cookson, P.D. Beer, P.T. Bishop, B. Thiebaut, J. Mater. Chem. 16 (2006) 209.
[40] G.H. Yang, L. Tan, Y.Y. Yang, S.W. Chen, G.Y. Liu, Surf. Sci. 589 (2005) 129.
[41] M.J. Hostetler, J.E. Wingate, C.J. Zhong, J.E. Harris, R.W. Vachet, M.R. Clark, J.D. Londono, S.J. Green, J.J. Stokes, G.D. Wignall, G.L. Glish, M.D. Porter, N.D. Evans, R.W. Murray, Langmuir 14 (1998) 17.
[42] T.W. Hansen, J.B. Wagner, P.L. Hansen, S. Dahl, H. Topsoe, C.J.H. Jacobsen, Science 294 (2001) 1508.
[43] S.W. Chen, R.W. Murray, S.W. Feldberg, J. Phys. Chem. B 102 (1998) 9898.
[44] H.A. Wierenga, L. Soethout, J.W. Gerritsen, B.E.C. Vandeleemput, H. Vankempen, G. Schmid, Adv. Mater. 2 (1990) 482.
[45] K. Majumdar, S. Hershfield, Phys. Rev. B 57 (1998) 11521.